Available online at www.sciencedirect.com

ScienceDirect

Procedia Structural Integrity 17 (2019) 992–1001

Structural Integrity Procedia

www.elsevier.com/locate/procedia

ICSI 2019 The 3rd International Conference on Structural Integrity

Experimental and numerical studies on the behaviour of fibre-reinforced composites subjected to soft impact loading

Haibao Liu[a], Jun Liu[a], Cihan Kaboglu[a], Hui Chai[b], Xiangshao Kong [c], Bamber R.K. Blackman[a], Anthony J. Kinloch[a,*], John P. Dear[a, *]

a Department of Mechanical Engineering, Imperial College London, South Kensington Campus, London SW7 2AZ, UK

b The First Aircraft Institute, No.1 East Renmin Road, Yanliang District, Xi'an, Shaanxi 710089, People's Republic of China

c Departments of Naval Architecture, Ocean and Structural Engineering, School of Transportation, Wuhan University of Technology, Wuhan, Hubei 430063, People's Republic of China.

Abstract

This paper presents detailed experimental and numerical studies on the behaviour of composite laminates subject to impact loading by soft objectives. In this research, gas-gun experiments employ woven carbon fibre reinforced poly (ether-ether ketone) (CF/PEEK) and gelatine projectiles to study the response of composite laminates under soft impact loading. A high-speed camera is employed to capture the deformation of the projectiles and a three-dimensional (3D) Digital Image Correlation (DIC) system is used to record the deformation of the impacted composite specimens. A numerical finite-element (FE) model, in which Hashin's theory is employed for composite modelling and Smooth Particle Hydrodynamics (SPH) method is used for modelling the gelatine projectile and is developed to simulate the soft impact on the composite laminates. The capability of the developed model is validated using the gas-gun experimental results. Good agreement has been shown between the predictions from using the FE model and the experimental results.

Peer-review under responsibility of the ICSI 2019 organizers.

Keywords: Thermoplastic composites; Soft impact; Digital Image Correlation; Numerical modelling

1. Introduction

With their increasing application in the aircraft industry, polymer-matrix fibre-reinforced composite materials have attracted much attention from both academia and industry. On the basis of an appropriate lay-up design, such

2452-3216
Peer-review under responsibility of the ICSI 2019 organizers.
10.1016/j.prostr.2019.08.132

composites can possess excellent in-plane properties, see Curtis et al. (1978) or Tsai and Hahn (2018). However, the effect of an impact load, e.g. a high-velocity soft impact, on the residual through-thickness properties is still a key safety concern for composite structures. With this in mind, gas-gun impact experiments have been widely used to evaluate the reliability of composite structures. Many efforts have been made by a number of researchers to investigate the behaviour of composite laminates subjected to impact loading by soft objects.

Heimbs and Bergmann (2012) conducted an experimental study on the response of composite specimens under high-velocity impact loads of soft-body gelatine projectiles. In their experiments, the composites were subjected to tensile and compressive loading before the impact experiments, to represent the realistic loading conditions of aircraft structures subjected to foreign-object impact. Based on the experimental data, the effects of a pre-load on the impact response of the composites were determined and it was found that the tensile and compressive pre-loading could influence the damage pattern observed in the composites. Zbrowski (2014) performed soft-body impact tests on the elements of a composite tail-plane component using a gas-gun system. The soft projectile was again made of gelatine. The head-on and off-centre collisions on elements of the tail-plane were studied using two high-speed cameras to record the interaction events between the projectile and the composite component. Damage inspection of the composite showed that the head-on collision significantly damaged the vertical tail-plane, but the off-centre collision caused only minor permanent deformation and, importantly, did not damage the leading edge of the component. Some publications, see Hou and Ruiz (2007) or Johnson and Holzapfel (2003), have shown that a mixture of 10% by weight gelatine and 90% by weight distilled water is one of the widely-used materials to conduct soft impact studies on composite materials.

In the present research, experimental and numerical studies on the impact behaviour of composite laminates subjected to soft impact are presented. For the experimental studies, the gelatine projectiles are employed to perform gas-gun impact tests on the composite target specimens. A high-speed camera is employed to capture the deformation and flow of the gelatine projectiles during the test and the deformations undergone by the composite specimens are recorded using a three-dimensional (3D) Digital Image Correlation (DIC) system. For the numerical studies, a FE model is developed, using 'Abaqus/Explicit 2017', to model the soft impact on the composite specimens. The main model for predicting the damage of the fibre-reinforced composites is based upon the Hashin damage approach, see Hashin and Rotem (1973), which has a higher computational efficiency than other sub-routine damage models. The soft gelatine projectile is modelled using the Smooth Particle Hydrodynamics (SPH) technique. The modelling results are then compared with the corresponding experimental results for model validation.

2. Projectiles, composite materials and test specimens

2.1. The soft projectiles

The ingredients used to prepare these projectiles were gelatine powder and distilled water. The gelatine powder was supplied by Honeywell Specialty, Germany. The gelatine projectiles had a nominal diameter of 23 mm and a nominal length of 45 mm. The geometry of the prepared projectiles are given in Fig. 1a. Table 1 shows the dimensions of the prepared gelatine projectiles.

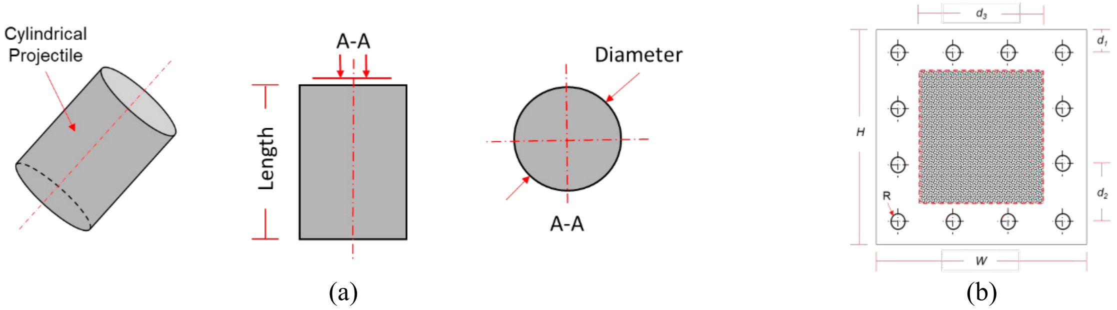

Fig. 1. The geometries: (a) the geometry of the gelatine projectiles and (b) the geometry of the composite specimens.

Table 1. Physical properties of the gelatine projectiles (Hou and Ruiz 2007; Johnson and Holzapfel 2003).

Projectile	Density (g/cm^3)	Mass (g)	Diameter (mm)	Length (mm)
Gelatine	1.06 ± 0.003	20 ± 0.5	23 ± 0.5	45 ± 0.5

2.2. The composite specimens

In this research, a woven-T300 carbon-fibre reinforced PEEK composite was evaluated. The woven carbon-fibre ply possessed a [0˚-90˚] architecture. These materials were supplied by Haufler Composites, Germany. An Out-of-Autoclave (OOA) manufacturing route was employed to consolidate the CF/PEEK prepregs. Composite specimens were manufactured from the composite panels, using a diamond saw and a floor-standing drill. The geometry of the composite specimens for the impact tests are given in Fig. 1b, where H and W are the specimen height and width, respectively, when mounted in the support fixture. The length, d_3, defines the size of the DIC pattern area. The length, d_1, defines the distance between the sample edge and the centre line of the holes and d_2 defines the distance between each of the holes. The radius of each hole is R. For the application of the DIC measurement system, the composite specimens were first painted on the rear-face using a white matt paint and then 'speckled' using a paintbrush to form the matt-black pattern for the DIC measurements. The edge length of the speckled area was defined as d_3. Table 2 gives all the dimensions of the specimens.

Table 2 Dimensions of the composite target test specimens.

Dimensions	W (mm)	H (mm)	d_1 (mm)	d_2 (mm)	d_3 (mm)	R (mm)
Values	140	140	16	36	70	5

2.3. Testing devices

A helium-propellant gas-gun, which has a four-litre pressure vessel and a three-metre-long barrel, was employed to accelerate the projectiles in the impact tests. The velocity of the projectile was adjusted by changing the pressure of the vessel. The incident velocity of the projectiles was measured using two pairs of infrared sensors located at the end of the barrel. New projectiles were employed for each impact test. The schematic of experimental set-up for gas-gun experiments is shown in Fig. 2. During the experiments, the target composite specimen was fixed by a specimen support. A 3D DIC system was used to measure the deformation of the specimens during impact experiments.

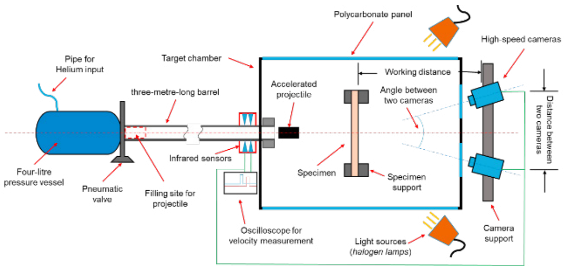

Fig. 2. Schematic of the experimental set-up for the gas-gun impact tests.

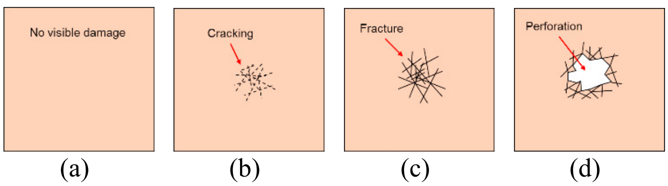

Fig. 3. Schematic of the post-test status: (a) no visible damage, (b) cracking, (c) fracture, and (d) perforation.

3. Experimental procedures

3.1. Gas-gun impact experiments

To study the response of the CF/PEEK composites subjected to soft impact loading, the CF/PEEK specimens were impacted using a gelatine projectile fired at four different impact velocities, and hence with different impact energy levels. The test details for these experiments are summarised in Table 3.

Table 3. Details for the gas-gun tests on the effects of the impact velocity on the impact response.

Test	Projectile	Projectile mass (g)	Impact velocity (m/s)	Impact energy (J)
GCP-I	Gelatine	20 ± 0.5	61 ± 2.5%	37 ± 5%
GCP-II	Gelatine	19 ± 0.5	75 ± 2.5%	53 ± 5%
GCP-III	Gelatine	20 ± 0.5	80 ± 2.5%	64 ± 5%
GCP-IV	Gelatine	20 ± 0.5	85 ± 2.5%	72 ± 5%

3.2. Damage inspection studies

After the impact experiments, a visual inspection was conducted on the composite specimens and photographs were taken of the rear-face of the post-impacted specimens. In general, the type of damage suffered by the composite specimens on the rear-face could be categorised as: (a) no visible damage present, (b) cracking observed, (c) fracture having occurred, and (d) perforation (i.e. penetration of the projectile through the specimen) having occurred. The main difference between 'type (b) cracking' and 'type (c) fracture' is whether there was fibre breakage observed. For 'type (b) cracking', this was defined as when cracks were only observed in the matrix. However, for 'type (c) fracture', fibre failure was also observed. Schematics of these descriptions are shown in Fig. 3.

4. Experimental results

4.1. Deformation of the gelatine projectile

Fig. 4 shows the deformation of the gelatine projectile recorded by a high-speed camera during an impact with the CF/PEEK composite specimen for an impact energy of 37 J. It was found that at the beginning of the impact event (i.e. t = 0.0 ms) the shape of the gelatine projectile was well preserved. However, in Fig. 4g for *t*=0.4 ms, the gelatine projectile can clearly be seen to be flowing freely after impact.

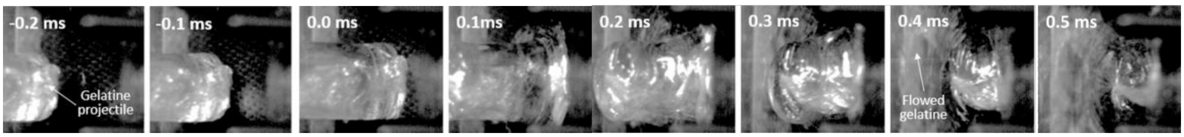

(a) (b) (c) (d) (e) (f) (g) (h)

Fig. 4. Deformation history of the gelatine projectile from 37 J impact energy level.

4.2. Digital Image Correlation (DIC) results for the CF/PEEK composite

The 3D DIC system was employed to measure the out-of-plane (OOP) displacement, on the rear-face of the composite specimens during the gas-gun experiments, Figures 11. The OOP displacement contours, corresponding to different times during the impact tests, were also obtained from the DIC results and shown in Fig. 5a. Similarly, the OOP displacements along the horizontal mid-section, during the loading and unloading of the specimen, were also obtained from the contour maps of the OOP displacement, and the results are shown in Fig. 5b, where the time interval is 0.025 ms during loading and unloading. The inset picture, on right, shows a horizontal solid line where the profile section is.

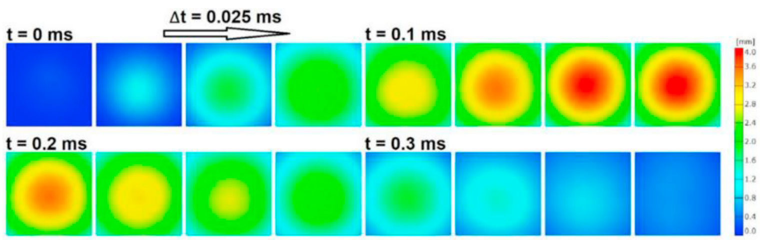

(a)

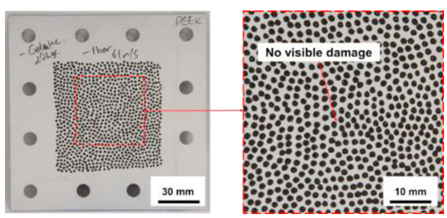

(a)

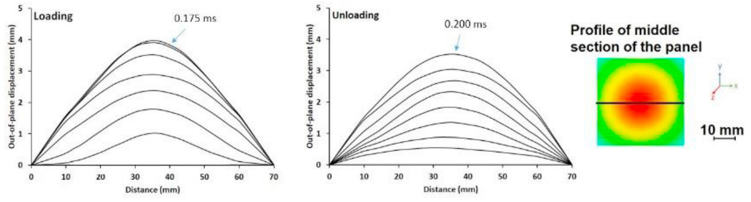

(b)

Fig. 5. CF/PEEK composite specimen impacted with a gelatine projectile at 37 J: (a) the OOP displacement contours and (b) the evolution of the OOP displacement profiles.

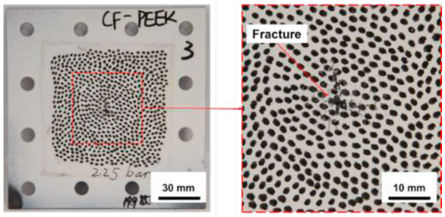

(b)

Fig. 6. Photographs of the rear-faces of the specimens after impacted at (a) 37 J and (b) 72 J energy level.

4.3. Post-impact assessment of the CF/PEEK composite

Representative photographs taken of the rear-faces of two of the gelatine-impacted CF/PEEK specimens are shown in Fig. 6, along with corresponding magnified images of the central area. In Fig. 6a, where the specimen has been impacted by a gelatine projectile with an energy of 37 J, there is no visible damage. The same observation of there being no visible damage was recorded for the tests conducted at impact energy levels of 53 J and 64 J. In contrast, the CF/PEEK composite specimen impacted at energy level of 72 J, has suffered fracture damage, with the cracking in the matrix mainly being confined to the central area of the specimen, Fig. 6b.

4.4. Summary of the results for the gelatine-impacted CF/PEEK specimens

The main experimental data obtained from the gelatine-impacted CF/PEEK specimens are summarised in Table 4. (It should be noted that due to fracture of the rear-face during 'Test GCP-IV', when an energy level of 72 J was used, no accurate value for the maximum major strain could be obtained from the DIC results for this test.) As the impact energy is steadily increased, the maximum major strain and maximum OOP displacement both increase in value. Further, the type of damage changes from there being no visible damage up to, and including, an impact energy of 64 J, but with fracture of the composite specimen being observed when an impact energy of 72 J is used.

Table 4. Main results for the CF/PEEK specimens after impact by the gelatine projectiles.

Test	Impact velocity (m/s)	Impact energy (J)	Type of post-impact damage	Maximum OOP displacement (mm)
GCP-I	61 ± 2.5%	37 ± 5%	(a) no visible damage	3.9 ± 3%
GCP-II	75 ± 2.5%	53 ± 5%	(a) no visible damage	4.2 ± 3%
GCP-III	80 ± 2.5%	64 ± 5%	(a) no visible damage	4.6 ± 3%
GCP-IV	85 ± 2.5%	72 ± 5%	(c) fracture	4.8 ± 3%

5. Numerical modelling

5.1. Finite-element (FE) model

A finite-element (FE) model was developed to model the soft impact on the composite test specimens, see Fig. 7a. In the FE model, the gelatine projectile was modelled using the Smoothed Particle Hydrodynamics (SPH) modelling technique. The SPH method is a meshless Lagrangian technique where the solid FE mesh for the gelatine impactor is replaced by a set of discrete interacting particles. The gelatine projectile was first modelled using 8-node linear-brick (C3D8R) elements, see Fig. 7b. However, upon initial contact of the projectile with the composite target specimen, these elements were converted to continuum particle (PC3D) elements, see Fig. 7b. The characteristic length for the PC3D elements was 0.5 mm, which was equivalent to half of the element size that was used for modelling the gelatine projectile with the CSD8R elements. The total mass of the projectile was equally distributed between all the 8-node linear-brick (C3D8R) elements or all the continuum particle (PC3D) elements.

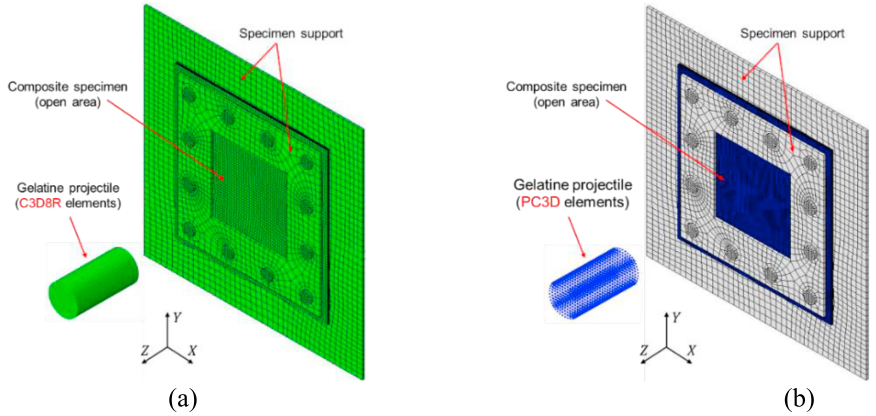

Fig. 7. FE model for (a) initial model with 8-node linear-brick (C3D8R) elements and (b) converted model of continuum particle (PC3D) elements for the gelatine projectile.

The Abaqus in-built Hashin damage model is only applicable to the unidirectional fibre-reinforced composite plies. Hence, the [0˚-90˚] woven carbon-fibre ply used for the CF/PEEK specimens was represented as two unidirectional-fibre sub-plies, joined at right angles to the fibre direction. Thus, in the FE modelling, two unidirectional-fibre sub-plies were first created, with the thickness of each of the unidirectional-fibre sub-plies (i.e. 0.125 mm) being equal to half that of the thickness of the equivalent [0˚-90˚] woven-fibre composite ply (i.e. 0.25 mm). These two unidirectional-fibre sub-plies were placed at right angles and then joined using 'tie constraints', to form a single equivalent [0˚-90˚] woven-fibre composite ply, which has the same in-plane properties as the actual woven-fibre composite ply that was used in the composite specimens. The elements employed for the composite target test specimens were 8-node quadrilateral in-plane general-purpose continuum shell (SC8R) elements, with an element size of 1 mm × 1 mm. The boundary conditions employed in the model were the same as those used in the gas-gun experiments. A general contact algorithm was used to govern the global contact in the numerical modelling and a friction coefficient of 0.2 was adopted for the global contact, see Liu et al. (2018).

5.2. Capturing the response of the projectile

The SPH approach was employed to model the behaviour of the gelatine projectile as a sub-routine in the 'Abaqus/Explicit 2017' code. In order to use the SPH method for capturing the response of the soft-gelatine projectile, an equation of state (EOS), with suitable input parameters, is required for the modelling of the gelatine projectiles. In this research, the Mie-Grüneisen EOS, which is linear in energy, was employed to define the coupled equations for pressure and internal energy of gelatine projectiles, see Abaqus 2017 documentation (2017). The input parameters, see Abdul Kalam et al. (2017) or Frissane et al. (2018), required for the numerical modelling of the gelatine projectiles are shown in Table 5.

Table 5. Properties required for modelling the projectiles.

Properties	Reference density	Dynamic viscosity	Reference speed of sound	Slope of the *Us* versus *Up* curve	Grüneisen ratio
Values	$1.06\ g/cm^3$	$1 \times 10^{-6}\ MPa \cdot s$	$c_0 = 1.45 \times 10^6\ mm/s$	$s = 1.87$	$\Gamma = 1.09$

5.3. The damage suffered by the composites

Damage initiation model. The main model for predicting the initiation of damage in 'Abaqus/Explicit 2017' is a sub-routine which is based upon the Hashin methodology, see Abaqus 2017 documentation (2017) or Hashin and Rotem (1973). In Hashin's damage model, four different types of damage mechanisms, which arise from tensile fibre failure, compressive fibre failure, tensile matrix failure and compressive matrix failure are employed to capture the initiation of damage in the unidirectional-fibre sub-plies. The material coordinate system in the unidirectional-fibre sub-ply was defined as the 1-2-3 coordinate system, where the longitudinal fibre direction is defined as the 11-direction and the transverse direction, perpendicular to the longitudinal fibre direction, is defined as the 22-direction. The general forms of the damage criteria in Hashin's approach to model the initiation of the above four different types of damage are given as, see Hashin and Rotem (1973):

Tensile fibre failure ($\hat{\sigma}_{11} \geq 0$): $$F_f^t = \left(\frac{\hat{\sigma}_{11}}{X^T}\right)^2 \quad (1)$$

Compressive fibre failure ($\hat{\sigma}_{11} < 0$): $$F_f^c = \left(\frac{\hat{\sigma}_{11}}{X^C}\right)^2 \quad (2)$$

Tensile matrix failure ($\hat{\sigma}_{22} \geq 0$): $$F_m^t = \left(\frac{\hat{\sigma}_{22}}{Y^T}\right)^2 \quad (3)$$

Compressive matrix failure ($\hat{\sigma}_{22} < 0$): $$F_m^c = \left(\frac{\hat{\sigma}_{22}}{2S^T}\right)^2 + \left[\left(\frac{Y^C}{2S^T}\right)^2 - 1\right]\frac{\hat{\sigma}_{22}}{Y^C} + \left(\frac{\hat{\tau}_{12}}{S^L}\right)^2 \quad (4)$$

In the above equations, the indices on the terms F_f^t, F_f^c, F_m^t and F_m^c represent the four types of damage of tensile fibre failure, compressive fibre failure, tensile matrix failure and compressive matrix failure, respectively. The parameters, X^T and X^C denote the tensile and compressive strengths in the longitudinal fibre direction, respectively. The terms Y^T and Y^C are the tensile and compressive strengths in the transverse direction, respectively; S^L and $S^T = Y^C/2$ denote the shear strengths in the longitudinal and transverse directions to the fibres, respectively; and $\hat{\sigma}_{11}$, $\hat{\sigma}_{22}$ and $\hat{\tau}_{12}$ are components of the effective stress tensor, $\hat{\sigma}$, that are used to evaluate the criteria. Further, the initiation of any interlaminar failure damage may be captured by a quadratic-stress criterion, given by:

$$\left(\frac{\langle t_{33}\rangle}{t_{33}^0}\right)^2 + \left(\frac{t_{31}}{t_{31}^0}\right)^2 + \left(\frac{t_{32}}{t_{32}^0}\right)^2 \leq 1 \quad (5)$$

where $t_i (i = 33, 31,32)$ represent the current normal and shear stresses and t_i^0 $(i = 33, 31,32)$ represent the normal and shear cohesive strengths, when the separation is either purely normal (i.e. the 33) direction to the interface or purely in the first shear (i.e. 31) or the second shear (i.e. 32) directions, respectively. The interlaminar damage is assumed to initiate when the above quadratic interaction function, involving the ratios of the stresses, reaches a value of one.

Damage evolution model. In both the intralaminar and interlaminar models, linear material softening was used to predict the post-damage initiation behaviour of the composite plies. A general form of the damage variable for a particular damage initiation mechanism is given by:

$$d = \frac{\varepsilon^f(\varepsilon - \varepsilon^0)}{\varepsilon(\varepsilon^f - \varepsilon^0)} \quad (6)$$

where $d = d_f^t$ for fibre tension failure, $d = d_f^c$ for fibre compression failure, $d = d_c^t$ for matrix tension failure, $d = d_m^c$ for matrix failure, and $d = d_{inter}$ for interlaminar failure, respectively. The strain, ε, is the equivalent strain in the composite ply. The strain values, ε^0 and ε^f, are the equivalent strains corresponding to initial failure and final failure, respectively. For more details, refer to the Abaqus 2017 documentation (2017).

5.4. Input parameters for the composite damage models

By employing the Hashin damage model as a sub-routine, the composite specimen may be simply defined as continuum shell elements and only the in-plane material properties are required for the numerical modelling. However, the values of the cohesive stiffness, maximum cohesive strength and the various fracture energies need to be inputted into the cohesive surface sub-routine. The relevant material properties of the CF/PEEK composites required for all the various sub-routines of the FE modelling studies may be found from the literature, see CYTEC (2012) or Liu et al. (2019, 2018, 2018) or Naderi and Khonsari (2013) or Turon et al. (2010) or Yoon and Sun (1991), and are given in Table 6.

Table 6. The values of the input parameters for the composite damage models.

Property	Unidirectional CF/PEEK sub-ply
Moduli (GPa)	$E_{11} = 127;\ E_{22} = 10.3;\ G_{12} = 5.7$
Poisson`s ratio	$\nu_{12} = 0.3$
Strength values (MPa)	$X^T = 2070;\ Y^T = 85;\ X^C = 1360;\ Y^C = 276;\ S^L = S^T = 186;$
Ply fracture energies (kJ/m^2)	$G_{Ic}\vert_{ft} = 218;\ G_{Ic}\vert_{fc} = 104;\ G_{Ic}\vert_{mt} = 1.7;\ G_{Ic}\vert_{mc} = 2.0$
Interlaminar fracture energies $^+$ (kJ/m^2)	$G_{Ic} = 1.7\ ;\ G_{IIc} = 2.0$
B-K component $^+$	$\eta_{BK} = 1.09$
Cohesive strengths (MPa)	$t_{33}^0 = 43;\ t_{31}^0 = t_{32}^0 = 50$
Cohesive stiffness (N/mm)	$k = 6.4 \times 10^5$

$^+$ Note: these properties are for interlaminar failure between two of the [0º-90º] woven-fibre plies.

6. Modelling results

6.1. Deformation of the gelatine projectile

The deformation history of the gelatine projectile obtained from the experimental studies and predicted using the FE model for an impact test conducted at an energy level of 37 J on the CF/PEEK composite, Fig. 8. The experimental results show that, after the initial contact with the composite specimen, the front of the gelatine projectile started to deform and flow to the periphery of the composite specimen. Correspondingly, the modelling results show a similar phenomenon, Fig. 8b. At a later stage of the impact event, Fig. 8e, most of the gelatine projectile has deformed, flowed and spread over the surface of the composite specimen, and again the modelling studies accurately capture this behaviour of the gelatine projectile.

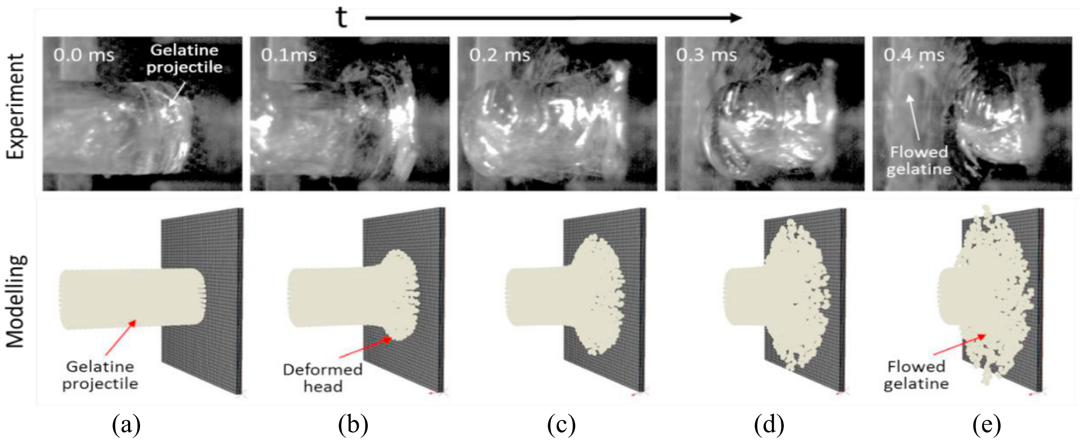

Fig. 8. Deformation of the gelatine projectile obtained from the experimental studies and as predicted from the numerical FE model for the CF/PEEK test specimens an impact energy of 37 J.

6.2. Deformation of the CF/PEEK composite

Based on the DIC results obtained from the experiment conducted at an impact energy of 37 J using the gelatine projectile, the major strain history and out-of-plane displacement history of the centre point for the rear-face of the composite test specimen can be extracted. The values of the maximum major strain and central OOP displacement predicted from the modelling studies are compared with the corresponding experimental results in Fig. 9a. The values of the predicted maximum major strain and central OOP displacement are 1.2% and 3.6 mm, respectively, which are only about 8% lower than the experimentally measured values. To further confirm the accuracy of the numerical FE model, the predicted central OOP displacement versus time trace was also compared with the corresponding experimental results, see Fig. 9b. It can be seen from the results in these figures that, although the modelling studies gave somewhat lower maximum values than the experimentally measured values, the general trend and overall response of the composite test specimen were predicted extremely well using the FE model.

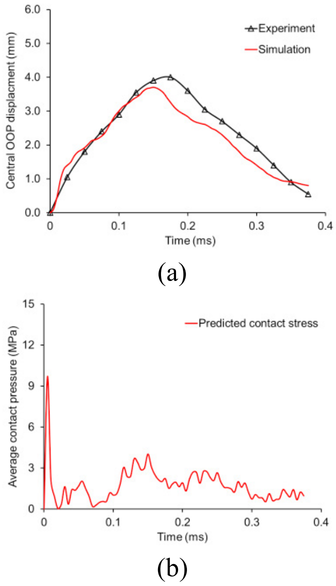

Fig. 9. The predicted and experimental results for 37 J impact: (a) the central OOP displacement versus time trace and (b) the predicted contact pressure.

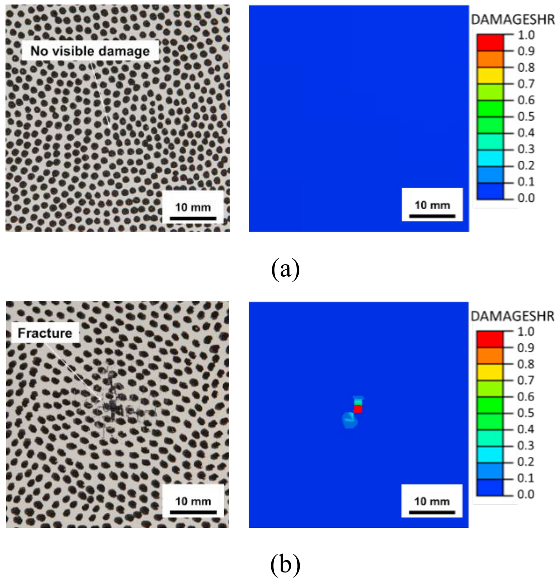

Fig. 10. The experimentally measured and predicted degrees of damage resulting in the rear-face of the CF/PEEK test specimens from using a gelatine projectile with (a) 37 J and (b) 72 J impact energies.

6.3. Damage in the CF/PEEK composite

The next step is to assess the capability of the numerical FE model that has been developed to predict the impact damage created in the composite by the impact event. The impact events were modelled at two impact energies of 37 J and 72 J. The experimental and predicted degrees of damage, which resulted in the CF/PEEK composite specimens, Figs. 10a and 10b, respectively. The term "DAMAGESHR" represents the predicted shear damage in the composites.

It was found that at an energy level of 37 J ('Test GCP-I') that the prediction from the numerical modelling studies was '(a) no visible damage', which is in agreement with the experimental results, Fig. 10a. When an impact energy level of 72 J ('Test GCP-IV') was modelled, failure was predicted to be present only in the central area of the gelatine-impacted CF/PEEK composite, Fig. 10b. The experimental results revealed that some damage had indeed occurred in this region of the composite. In addition, the extent of the damage, as determined from the post-impact experimental observations on the composite specimen, is accurately predicted by the numerical studies.

Conclusions

This paper has focussed on experimental and numerical studies of the response of polymer-matrix fibre-reinforced composites under impact loading by a soft objective. A high-speed camera was used to record the deformation of the projectile during the impact event. The recorded frames showed that the gelatine projectile behaved as a viscoelastic-plastic fluid. The gas-gun tests were performed using woven carbon-fibre reinforced poly (ether-ether ketone) (CF/PEEK) composite specimens, using the gelatine projectiles, at four impact energy levels, to investigate the behaviour of composite laminates under soft impact loading. Then, a finite-element (FE) numerical model was developed to predicting the behaviour of the projectile and the composite specimens, during the impact event. This numerical model enabled (a) the deformation, (b) the initiation of damage, and (c) the evolution of such damage in the composite target specimens to be predicted, as well as the deformation and flow behaviour (and the contact pressure) of the projectile. The results from the numerical studies have been found to be in very good agreement with the experimental results.

Acknowledgements

The strong support from the Aviation Industry Corporation of China (AVIC) Manufacturing Technology Institute (MTI), the First Aircraft Institute (FAI) and the Aircraft Strength Research Institute (ASRI) for this funded research is much appreciated. The research was performed at the AVIC Centre for Structural Design and Manufacture at Imperial College London, UK.

References

Curtis, P.T., Bader M.G., Bailey JE., 1978. The Stiffness and Strength of a Polyamide Thermoplastic Reinforced with Glass and Carbon Fibres. Journal of Materials Science 13, 377–90.

Tsai, S.W., Thomas H., 2018. Introduction to Composite Materials Science. Routledge.

Heimbs, S., Tim B., 2012. High-Velocity Impact Behaviour of Prestressed Composite Plates under Bird Strike Loading. International Journal of Aerospace Engineering 2012, 1–11.

Zbrowski, A, 2014. Experimental Tests Concerning the Impact Resistance of a Tailplane. Archives of Civil and Mechanical Engineering 14, 53–60.

Johnson, A.F., Martin H., 2003. Modelling Soft Body Impact on Composite Structures. Composite Structures 61, 103–13.

Hou, J. P. and Ruiz C., 2007. Soft Body Impact on Laminated Composite Materials. Composites Part A: Applied Science and Manufacturing 38, 505–15.

Hashin, Z., Rotem A., 1973. A Fatigue Failure Criterion for Fiber Reinforced Materials. Journal of Composite Materials 7, 448–64.

Liu, H., Falzon B.G., Catalanotti G., Tan W., 2018. An Experimental Method to Determine the Intralaminar Fracture Toughness of High-Strength Carbon-Fibre Reinforced Composite Aerostructures. The Aeronautical Journal 122, 1352–70.

Abaqus 2017 documentation, 2017. Dassault Systèmes. Providence, Rhode Island, USA.

Frissane, H., Taddei L., Lebaal N., Roth S., 2018. SPH Modeling of High Velocity Impact into Ballistic Gelatin. Development of an Axis-Symmetrical Formulation. Mechanics of Advanced Materials and Structures 3, 1–8.

Abdul Kalam S, Vijaya Kumar R., Ranga Janardhana G., 2017. SPH High Velocity Impact Analysis-Influence of Bird Shape on Rigid Flat Plate. Materials Today: Proceedings 4, 2564–72.

Naderi M., Khonsari M.M., 2013. Stochastic Analysis of Inter- and Intra-Laminar Damage in Notched PEEK Laminates. Express Polymer Letters 7, 383–95.

Liu H., Falzon B.G., Tan W., 2018. Experimental and Numerical Studies on the Impact Response of Damage-Tolerant Hybrid Unidirectional/Woven Carbon-Fibre Reinforced Composite Laminates 136, 101-118.

Turon A., Camanho P.P., Costa J., Renart J., 2010. Accurate Simulation of Delamination Growth under Mixed-Mode Loading Using Cohesive Elements: Definition of Interlaminar Strengths and Elastic Stiffness. Composite Structures 92, 1857–64.

Liu H., Falzon B.G., Tan W., 2018. Predicting the Compression-After-Impact (CAI) Strength of Damage-Tolerant Hybrid Unidirectional/Woven Carbon-Fibre Reinforced Composite Laminates. Composites Part A: Applied Science and Manufacturing 105, 189–202.

Liu, H., Falzon B.G., Li S., Tan W., Liu J., Chai H., Blackman B.R.K., and Dear J.P., 2019. Compressive Failure of Woven Fabric Reinforced Thermoplastic Composites with an Open-Hole: An Experimental and Numerical Study. Composite Structures 213, 108–17.

CYTEC, 2012. APC-2-PEEK Thermoplastic Polymer.

Yoon K.J., Sun C.T., 1991. Characterization of Elastic-Viscoplastic Properties of an AS4/PEEK Thermoplastic Composite. Journal of Composite Materials 25, 1277–96.